Spectroscopy of positively and negatively buckled domains on Si(111)-2 × 1

K. Löser, M. Wenderoth,* T. K. A. Spaeth, J. K. Garleff, and R. G. Ulbrich
IV. Physikalisches Institut der Universität Göttingen, Friedrich-Hund-Platz. 1, 37077 Göttingen, Germany

M. Pötter and M. Rohlfing
Department of Physics, University of Osnabrück, 49069 Osnabrück, Germany
(Received 26 March 2012; revised manuscript received 23 May 2012; published 8 August 2012)

The influence of the buckling type of the Si(111)-2 × 1 surface on the electronic structure is studied with high-resolution scanning tunneling microscopy and scanning tunneling spectroscopy and compared to *ab initio* calculations. We utilize the multitude of domain boundaries to identify differently buckled domains. $I(V)$ measurements with high spatial and energetic resolution show the electronic structures of the two buckling types. We determine the position of the surface bands in the band gap of the bulk silicon and relative to each other. The high spatial resolution provides insight into the crossover from one buckling type to the other at the domain boundaries.

DOI: 10.1103/PhysRevB.86.085303 PACS number(s): 68.37.Ef, 73.20.At, 68.35.B−

I. INTRODUCTION

Semiconductor systems offering two metastable states with similar total energies close to the ground state are of increasing interest due to potential applications for nanoscale devices such as a rewritable nanoscale memory.[1] Appelbaum *et al.* considered the Si(001) surface where differently tilting dimers lead either to a $c(2 \times 4)$ or to a $p(2 \times 2)$ reconstruction. The same applies for the Ge(001) surface. The reconstruction can be reversibly changed from $c(2 \times 4)$ to $p(2 \times 2)$ by applying different voltages and tunneling currents.[2–5] Calculations confirm the influence of electric fields and charge injection on the stability of the two reconstructions.[6,7]

Only recently it was shown that the Si(111)-2 × 1 surface belongs to these semiconductor systems where different atomic configurations with similar total energies close to the ground state coexist.[9] Below room temperature, the cleaved Si(111) surface undergoes a 2 × 1 reconstruction. This reconstruction is usually described with the π-bonded chain model by Pandey in which the π-bonded chains buckle to reduce the total energy.[10] There are two different buckling configurations (Fig. 1) for which calculations predict similar total energies and surface band structures.[8]

Until a short while ago, experimentalists and theoreticians assumed that all π-bonded chains on a surface were buckled in the same way. Nie *et al.* have shown in room-temperature scanning tunneling microscopy (STM) measurements that the π-bonded chains of the Si(111)-2 × 1 surface are positively buckled, in contrast to Ge(111)-2 × 1, which exhibits negative buckling of the π-bonded chains.[11] This agrees well with our former calculations, where we find positive buckling favorable for Si(111)-2 × 1 while Ge(111)-2 × 1 should show negative buckling.[12]

Bussetti *et al.* were able to prove the coexistence of both buckling types for highly n-doped samples and at low temperatures. They assume that the n-type doping is essential for the formation of domains of π-bonded chains with negative buckling in addition to the otherwise preferred positive buckling. The highly n-doped samples may reduce the total energy by occupying the empty states of the negatively buckled π-bonded chains.[9]

In the case that there is only one buckling type at the sample, it is difficult to determine the buckling type directly in STM measurements as the relative positions of the atoms are identical for the first three atomic layers, seen from above the surface.

In this paper, we use domain boundaries to determine whether two adjacent domains are buckled differently or likewise. In STM measurements at room temperature as well as at 6 K, we find domains of positively buckled π-bonded chains as well as domains with negative buckling on multidomain Si(111)-2 × 1 surfaces. The electronic structure of differently buckled domains is studied with high spatial and energetic resolution. This allows us to determine not only the band gaps of the two buckling types, but also the crossover between the two buckling types at domain boundaries, parallel and perpendicular to the chains. Our *ab initio* calculations of the band structure for both buckling types are used for comparison with the experimental results.

II. EXPERIMENTAL AND THEORETICAL DETAILS

A. Experiment

Clean Si(111) surfaces were prepared by cleaving Czochralski-grown n-type silicon single crystals (6×10^{18} phosphorus atoms/cm^3) in the $[0\bar{1}1]$ direction. The cleavage was done at room temperature in ultrahigh vacuum (UHV) at a base pressure of 5×10^{-11} mbar. The samples were mounted into the custom-made Besocke-type STM without breaking the UHV. High-resolution STM and scanning tunneling spectroscopy (STS) measurements at temperatures of 6 and 300 K were performed with tungsten tips which were electrochemically etched and further prepared in UHV (for details, see Ref. 13).

B. Theory

For a direct comparison with the experiments, we have carried out *ab initio* calculations of the surface, employing a combination of density-functional theory (DFT) and many-body perturbation theory (MBPT) (for details, see Garleff *et al.*[13]). Starting from a positively or negatively buckled Pandey chain

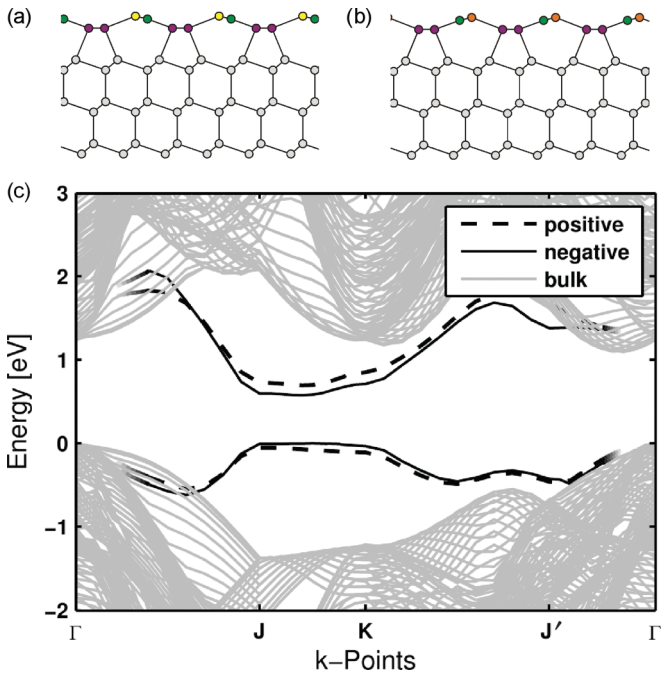

FIG. 1. (Color online) Equilibrium structures of positively (a) and negatively (b) buckled π-bonded chains (Ref. 8). (c) Calculated electronic surface dispersion for positive (dashed lines) and negative (solid lines) buckling, in comparison with the projected bulk band structure (gray), resulting from the GW band-structure theory (see text).

[see Figs. 1(a) and 1(b)], DFT total-energy minimization yields the structural details of each structure.

The chain atoms have threefold coordination, only, instead of the tetrahedrally fourfold coordination of bulk atoms, yielding one dangling bond per chain atom. Within the 2×1 unit cell, these dangling bonds form two surface bands. As a consequence of the (positive or negative) buckling of the chain, the gap between the two surface bands opens up at the Brillouin-zone boundary [see Fig. 1(c)]. This gap opening constitutes the driving force of the buckling. The accurate evaluation of the band-structure energies is not possible within DFT, but requires the inclusion of quasiparticle (QP) corrections that originate from exchange and correlation effects among the electrons. This is done within the GW approximation (GWA) of the electron self-energy operator (see Garleff *et al.*[13] for details). In the present system, QP corrections are relevant both for the absolute value of the fundamental surface gap and for the position of the surface bands relative to the bulk states. The surface valence band state of the π-bonded chains (π_{SVB}), formed from p_z-like orbitals at the up atoms, is lower in energy than the surface conduction band state (π_{SCB}), which is mainly formed from p_z-like orbitals at the down atoms. Consequently, the π_{SVB} band is filled, while the π_{SCB} band is empty. This constitutes a semiconducting band structure. However, the differences between positive and negative buckling (i.e., the orientation of the buckling relative to the deeper layers of the material) causes subtle differences in the electronic structure, yielding slight but measurable differences in the surface band structure [see Fig. 1(c) and Bussetti *et al.*[9]]. Compared to positive buckling, the occupied (empty) dangling-bond band of the negative buckling is higher (lower) in energy by 0.09 eV. The surface band gap for positive (negative) buckling amounts to 0.75 eV (0.58 eV). Note that Fig. 1(c) does not easily allow for a comparison of electronic levels on different domains relative to each other (on an absolute energy scale), which might be influenced by doping and space-charge effects. As shown below, the calculated surface band gap is trustworthy (in particular, its closing by 0.17 eV when changing the buckling from positive to negative), but absolute surface band levels must be treated with care. Concerning the agreement between theory and experiment in the change of the band gap between positive and negative buckling, note that our calculated band-structure data may suffer from inaccuracies related to the approximative nature of the GW approach, as well as possible inaccuracies in the geometric structures (resulting from DFT geometry optimization). The agreement of our calculated gap change (170 meV) with the measured one (230 meV) is within these inaccuracies.

III. RESULTS AND DISCUSSION

The topography image [Fig. 2(a)] shows the typical π-bonded chains of the Si(111)-2 × 1 surface with atomic resolution. The bright spots are adsorbates, which mainly occur after a time in room-temperature measurements and are absent

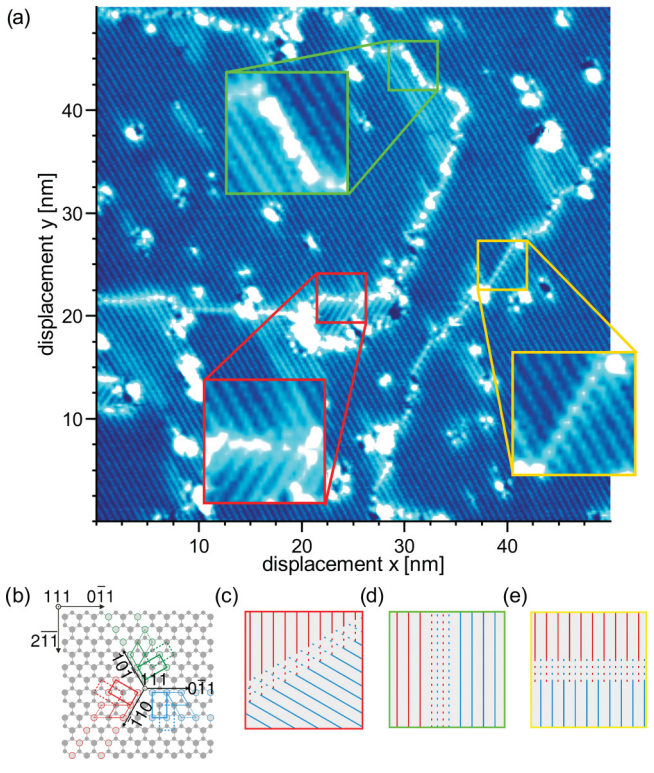

FIG. 2. (Color online) (a) STM topography showing domain boundary type I (red), type II (green), and type III (yellow) [$V_{\mathrm{bias}} = -1$ V; $I_t = 0{,}1$ nA; $T = 300$ K]. (b) Atomic positions of the six configurations, green: $[10\bar{1}]$ direction; blue: $[0\bar{1}1]$ direction; red: $[\bar{1}10]$ direction. Solid and dashed lines: two possibilities of up-atom positions with displacement of half a 2×1 unit cell, (c)–(e) schemes of type-I (c), type-II (d), and type-III (e) domain boundaries.

in the measurements at 6 K. The bright, irregular lines are domain boundaries, which present extended defects of the 2×1-reconstructed surface.

To identify differently buckled domains, we make use of these domain boundaries separating differently oriented π-bonded chains. The π-bonded chains can run in $[0\bar{1}1]$, $[10\bar{1}]$, and $[\bar{1}10]$ directions due to the threefold symmetry of the nonreconstructed Si(111)-1×1 surface. Together with the two equivalent positions of upper and lower chains with a displacement of half a 2×1 unit cell with respect to each other, there are six different possibilities for the atoms to be arranged with respect to the unreconstructed Si(111) surface [Fig. 2(b)]. If one adds the two different buckling types, there are all in all 12 different configurations which are separated by three main types of domain boundaries.

Type I of the domain boundaries covers all configurations in which the π-bonded chains are rotated by 120° with respect to each other in the two domains [Fig. 2(c)]. Boundaries of types II and III both separate domains in which the π-bonded chains run in the same direction but have either a displacement of half a unit cell or different buckling types or both. In the case of type-II boundaries, the π-bonded chains run parallel to the boundary [Fig. 2(d)], while type-III boundaries cut the chains [Fig. 2(e)].

In our investigations of Si(111)-2×1 surfaces at 6 K and at room temperature, we found all three types of domain boundaries on multidomain surfaces. In the red framed area of Fig. 2(a), two domains with rotated π-bonded chains meet in a type-I domain boundary, while the green framed area shows a type-II domain boundary, running parallel to the π-bonded chains. In the yellow framed area, a type-III boundary that cuts the π-bonded chains can be seen. Here, the displacement of the π-bonded chains of the two domains is clearly visible.

Closer examination of the type-III domain boundaries in STM measurements at room temperature and at 6 K revealed π-bonded chains meeting with different displacements of the up atoms (Fig. 3). We compare the displacement of the up atoms of a π-bonded chain in one domain relative to the neighboring π-bonded chains in the second domain. In many cases, the distance is the same to two neighboring π-bonded chains which means that the up atoms are displaced by exactly half a 2×1 unit cell [Fig. 3(a)].

However, there are also type-III domain boundaries where the displacement to one neighboring chain is twice as much as to the neighboring π-bonded chain on the other side. While the centered meeting up atoms can be easily explained by a model with only one buckling type in both domains [Figs. 3(a) and 3(c)], another model must be taken into account to describe the π-bonded chains meeting with the up atoms in the distance relation of 0.42 nm versus 0.22 nm. By assuming that the π-bonded chains in one domain are buckled positively while the other domain consists of negatively buckled π-bonded chains, this distance relation of 0.42 nm versus 0.22 nm can be explained perfectly [Figs. 3(b) and 3(d)]. Our DFT-optimized structures yield 0.447 and 0.218 nm for these spatial offset values. In this way, it is possible to see in the topography measurement whether two domains are buckled likewise or differently.

To further investigate the different buckling types, we performed CITS (current imaging tunneling spectroscopy)

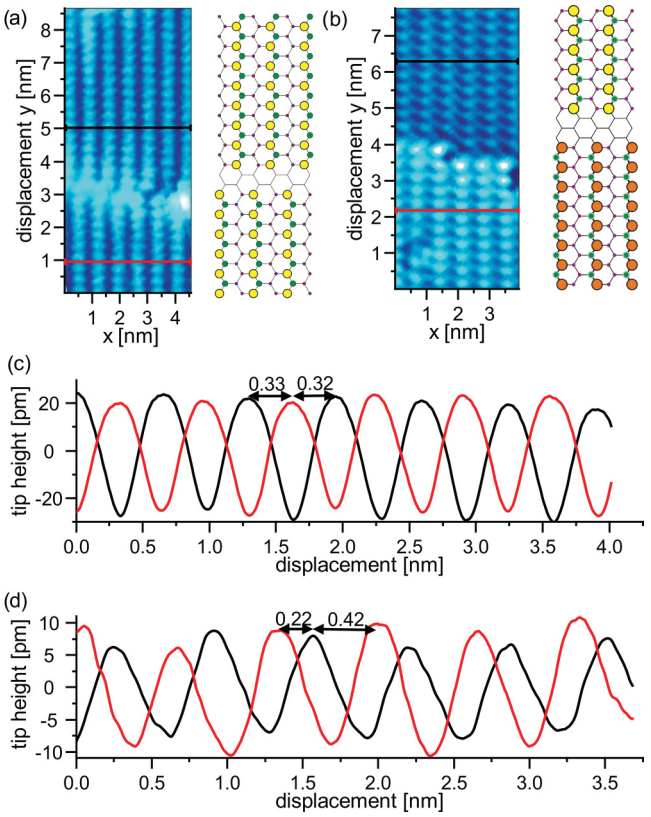

FIG. 3. (Color online) (a), (b) Topography images of type-III domain boundary separating two domains with same (a) and with different (b) buckling types [$V_{\text{bias}} = -1$ V; $I_t = 0.1$ nA; $T = 300$ K]. At the right side of the images, the respective surface models are illustrated: big yellow circles, up atoms (buckling type A); big orange circles, up atoms (buckling type B); green circles, down atoms; purple circles, atoms of lower chain. (c), (d) Averaged height profiles of lower (red) and upper (black) domains [see corresponding lines in topography images (a) and (b)].

measurements of multidomain areas of the Si(111)-2×1 surface which reveal differences in the electronic structure of differently buckled domains (Fig. 4). Figure 4(a) shows the topography data of a large domain with one type of buckling enveloping a smaller domain with the other buckling type. The current maps at different voltages display the differing integrated densities of states of the domains. At a voltage of $V_{\text{bias}} = -1.0$ V, all domains show the same tunneling current [Fig. 4(b)], while at $V_{\text{bias}} = -0.3$ V the small domain displays a much higher tunneling current due to an increased density of states at this voltage [Fig. 4(c)]. This situation is reversed for positive voltages when the surrounding domains have a higher tunneling current [Fig. 4(d)].

To examine these differences in the electronic structure and the crossover between the buckling types in more detail, we use high-resolution $I(V)$ measurements of different domain boundaries at 6 K and at room temperature (Figs. 5 and 6). The band gaps of the differently buckled domains are determined using single dI/dV spectra. In spatial profiles of the $dI/dV(x,y,U)$ data set, the variations of the band gap E_G, the valence and the conduction bands along a line in the topography data, are revealed.

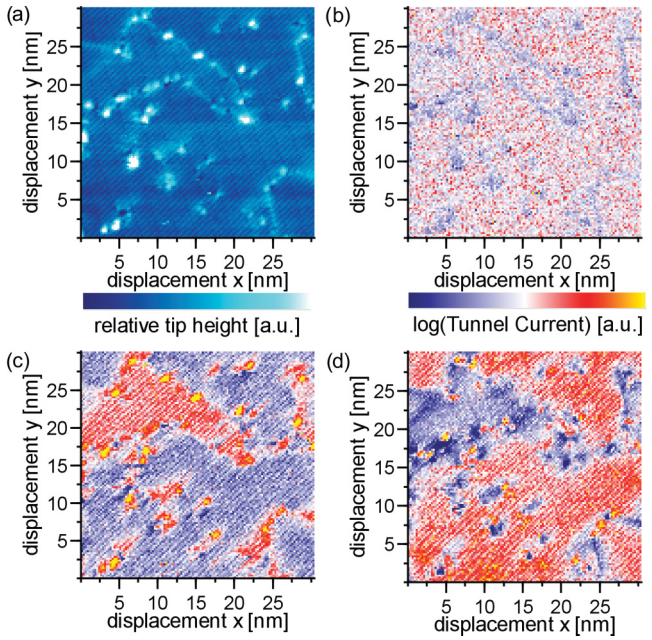

FIG. 4. (Color online) CITS data of multidomain Si(111)-2 × 1 surface. (a) Topography image [$V_{\text{bias}} = -1$ V; $I_t = 0{,}15$ nA; $T = 300$ K]. (b)–(d) Current map at a voltage of -1.0 V (b), -0.5 V (c), and $+1.0$ V (d). The contrast is due to different buckling types in the domains. Note that one color depicts different current values in the individual figures as the current ranges differ a lot between the maps at different voltages.

Figure 5 shows data of a spectroscopy map taken at 6 K that includes three domains which are separated by a type-II domain boundary [between left (p) and right (n_1) sides in the upper part of Figs. 5(a) and 5(b) as well as a type-III domain boundary [between upper (p and n_1) and lower (n_2) parts of Figs. 5(a) and 5(b)]. In the topography image [Fig. 5(a)], the type-II boundary is visible in a slightly lighter color of the two π-bonded chains that form the boundary, while the type-III boundary is visible as bright line cutting the π-bonded chains.

At low temperatures of 6 K, the different band gaps are well distinguished, as single dI/dV spectra from the different domains show [Fig. 5(c)]. Due to the high negative doping, the Fermi energy lies at the lower edge of the surface conduction band for both buckling types in agreement with photoemission studies by Himpsel *et al.*[14] The band gap of the π-bonded chains with positive buckling has a width of $E_{Gp} = 520\,(20)$ mV, while the π-bonded chains with negative buckling exhibit a smaller band gap of $E_{Gn} = 290\,(20)$ mV. The value for positive buckling agrees well with early spectroscopic measurements by STM of the Si(111)-2 × 1 surface.[15] Both values are in qualitative agreement with the results by Bussetti *et al.*[9] Our calculated surface band gaps amount to $E^t_{Gp} = 750$ mV and $E^t_{Gn} = 580$ mV, showing the same band-gap reduction when changing the buckling from positive to negative. Note that our measured band gaps are systematically smaller than the calculated ones. In the experiment, the tail of the spectrum makes it difficult to assign absolute values to band positions. Furthermore, our theoretical approach does not consider spectral broadening (and possibly level shifts) from electron-phonon interaction (which might account for 100 meV or more in the present case[16]). Also, the n-type doping might reduce the absolute size of the gap, which can not be considered in the present theory.

Figure 5(e) shows a spatial profile of the $dI/dV(x,y,U)$ data set across the type-III boundary between the two domains with negative buckling [n_1 and n_2, red line in Fig. 5(a)]. Both domains have the same band gap E_{Gn}. The spatial profile of the $dI/dV(x,y,U)$ data set across the type-III domain boundary separating two domains of different buckling types [p and n_2, Fig. 5(f)] was taken at the position of the yellow line in Fig. 5(a). The variation in the dI/dV spectra resembles the band structure of a heterostructure of materials with different band gaps. The domain on the left side has the larger band gap E_{Gp} of π-bonded chains with positive buckling, while the right domain shows the significantly smaller band gap E_{Gn} of negative buckling.

The type-II boundary [Fig. 5(d)] between domains with different buckling types [p and n_1, green line in Fig. 5(a)] affects only the two π-bonded chains that form the boundary itself, while the energetic position of the bands in the neighboring chain remains undisturbed. This confirms that the interaction between neighboring π-bonded chains inside a given domain is negligible.[17]

The room-temperature spectroscopy maps in Fig. 6 contain type-III domain boundaries, one with two positively buckled domains [Figs. 6(a) and 6(b)], the other with both buckling types [Figs. 6(c) and 6(d)]. The band gaps, extracted from single dI/dV spectra, taken at various sites and samples, differ more than the low-temperature results. The band gap for positively buckled domains is larger than for negative buckling. Approximate values are $E_{Gp} = 300{-}400$ mV for positively buckled π-bonded chains and $E_{Gn} = 200{-}250$ mV for π-bonded chains with negative buckling [Fig. 6(e)].

The spatial profile of the $dI/dV(x,y,U)$ data set across the type-III domain boundary separating two positively buckled domains has the larger band gap E_{Gp} in both domains [Figs. 6(a) and 6(b)], while the spatial profile of the $dI/dV(x,y,U)$ data set across the type-III boundary with both buckling types looks similar to the one at low temperatures [Fig. 6(c)] with the smaller band gap E_{Gn} in the left domain with negative buckling and E_{Gp} in the positively buckled right domain.

Going a step further in the analysis of single dI/dV spectra gives us access to the exact positions of the surface bands for both buckling types within the bulk band gap [Fig. 7(a)]. The determination of the positions is not intuitive because of diverse configurations leading to different energetic positions of the bulk bands in relation to E_F at the surface. We assume that the sample is in equilibrium (const E_F), and that we can neglect the effect of tip-induced band bending. This assumption is supported by $I(V)$ measurements where we find no significant impact of V_{bias} and I_t on the spectroscopic signatures. At first, we describe for one buckling type (e.g., positive buckling) the potential landscape perpendicular to the surface within the rigid band model. For high n-type doping with phosphorus in the bulk, E_F is located in the shallow donor band ~45 meV below the bulk conduction band.[18] At the surface, there is a surface state within the bulk band gap. The high density of states of the conduction surface band in combination with a

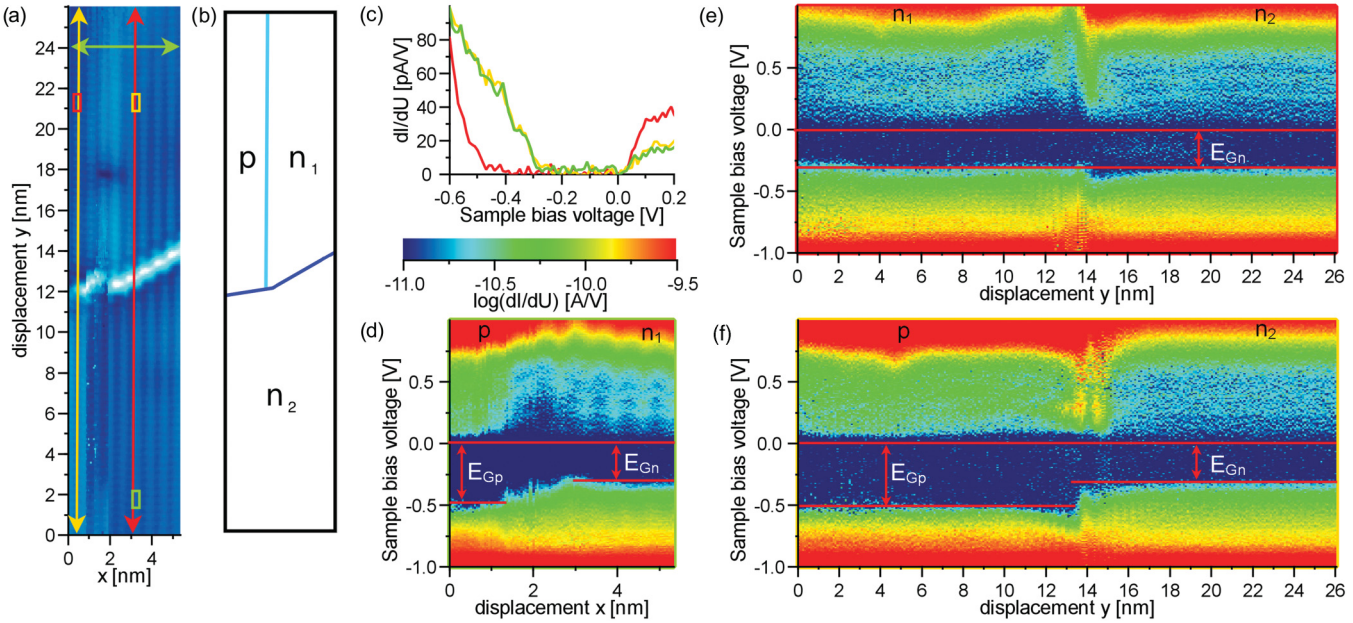

FIG. 5. (Color online) STS data of measurements at 6 K. (a) Topography image: red, yellow, and green boxes mark positions of dI/dV single spectra (c); red, yellow, and green lines mark positions of spatial profiles of the $dI/dV(x,y,U)$ data set (d)–(f) [$V_{\text{bias}} = -1$ V; $I_t = 0{,}1$ nA; $T = 6$ K]; (b) sketch of domains (p: positively buckled domains; n_1 and n_2: negatively buckled domains) and domain boundaries (light blue: type-II boundary, dark blue: type-III boundary); (c) single dI/dV spectra of different domains in (a): red, positive buckling (p); yellow, negative buckling (n_1); and green, negative buckling (n_2); (d)–(f) spatial profiles of the $dI/dV(x,y,U)$ data set across type-III boundary with same [(e), red line]/different [(f), yellow line] buckling type in the two domains and type-II boundary [(d), green line], red lines mark positions of band edges.

large charge accumulation as a result from the n-doped bulk leads to a quasipinning of E_F near the surface conduction band minimum.[14] This situation is comparable to a Shottky barrier with barrier height $\Delta E_{\text{SC}p-\text{BC}} - 0.045$ eV $= 0.355$ eV with $\Delta E_{\text{SC}p-\text{BC}} = 0.4$ eV according to our calculations [Fig. 1(c)]. The width of the resulting space charge region is $\lambda_{Dp} = 9.0$ nm and the surface charge density $\rho_p = 5.4 \times 10^{12}$ cm^{-2} [Fig. 7(b)]. For negative buckling, with $\Delta E_{\text{SC}n-\text{BC}} = 0.485$ eV according to our calculations [Fig. 1(c)], the Shottky barrier $\Delta E_{\text{SC}n-\text{BC}} - 0.045$ eV $= 0.440 = 0.440$ eV is higher than for positive buckling. This leads to a wider space charge region with $\lambda_{Dp} = 10.0$ nm and higher surface charge density $\rho_n = 6.0 \times 10^{12}$ cm^{-2} at negatively buckled domains [Fig. 7(c)]. In the last step, we consider the lateral coexistence of negative and positive buckled areas including the resulting domain boundary. At a large distance from the domain boundary, the surface conduction bands minimum are both close to E_F and the bulk bands at the energetic positions of 0.4 eV (positive buckling) and 0.5 eV (negative buckling), respectively, above E_F [Fig. 7(d)]. Directly at the boundary position, the two electronic systems align similar to contact between two different semiconductors, e.g., GaAs/AlAs resulting in *surface band offsets* at the boundary line and a three-dimensional (3D) space charge layer in the vicinity. The latter electrostatic problem is defined by the charge distribution in the surface layer and the space charge layer in the bulk. The precise nature of this junction depends on the nature of edge states resulting from broken symmetry at the boundary and perhaps on the "electron affinity" of the two systems. The investigation of this junction is not part of this paper, but from Figs. 5(e) and 5(f) we can define a length scale at which the contact region may be neglected: at a distance of more than 5 nm apart from the domain boundary there is no significant influence on the electronic structure.

In the following analysis, we use a signature of the bulk bands within our $I(V)$ spectra as reference for all energetic positions. In the voltage regime of our $I(V)$ measurements between -1.0 and 1.0 V, we can distinguish different tunneling channels [Fig. 8(a)]. For higher voltages, the main contribution to the tunneling current comes from the bulk bands (yellow). At small positive voltages, the major tunneling channel is provided by tunneling into the empty states of the surface conduction band (green). The fraction of tunneling into the tails of the bulk conduction band is very small and adds no distinct signature to the dI/dV spectrum. The situation is similar for negative voltages between the edge of the surface conduction band and higher negative voltages up to 0.8 V. There, the main component of tunneling current stems from tunneling out of the surface valence band with only a small part of tunneling current from the bulk valence band. In the surface band gap (blue), there is only a small amount of tunneling current due to tunneling out of the filled states of the surface conduction band.

The fraction of tunneling current due to tunneling through the space charge region is negligible,[19] but leads to a smoothed onset of current into the bulk conduction band instead of a sharp step. In combination with the small density of states (DOS) of and the low transmission into the bulk conduction

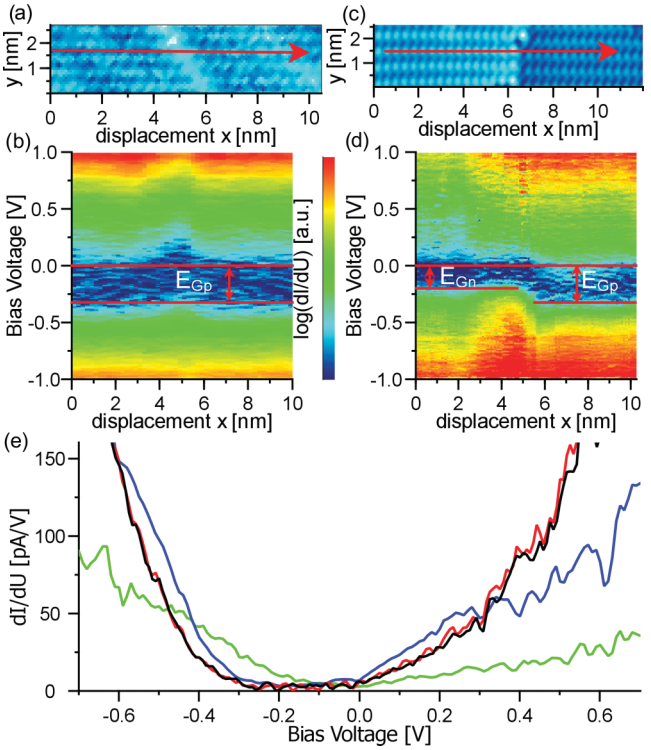

FIG. 6. (Color online) STS data of room-temperature measurements. (a), (c) Topography images across type-III domain boundary with same (a)/negative (left side) and positive (right side) (c) buckling type on both sides. The red line marks position of spatial profiles of the $dI/dV(x,y,U)$ data set (b) and (d) [$V_{\text{bias}} = -1$ V; $I_t = 0.1$ nA; $T = 300$ K]. (b), (d) Spatial profiles of the $dI/dV(x,y,U)$ data set along red lines in (a) and (c), red lines mark positions of band edges. (e) Single dI/dV spectra of the different domains in (a) and (c).

band states at the edge of the Brillouin zone, this leads to masking of the bulk band edges by the surface bands and thus to a seemingly larger gap of the bulk bands. For our analysis, this means that we can not use the edges of the bulk bands as reference. Instead, the strong increase in dI/dV signal at higher voltages is considered. In addition, at the setpoint of our measurements ($V_{\text{bias}} = -1.0$ V; $I_T = 0.1$ nA), the distance between sample and tip is different for the two buckling types, due to the unequal energetic position of the bulk bands in relation to E_F and the resulting difference in the integrated density of states at the setpoint voltage. To compare the band positions of the different buckling types, it is necessary to "adjust" the spectra.

In the first step, we adjust signal height and energetic position of the dI/dV spectra assuming that the bulk bands are identical for negative and positive buckling [Figs. 8(b)–8(d)]. To compensate the differing distances, first the dI/dV values of the curve for negative buckling are multiplied with 1.87 matching the height of the dI/dV signal from the surface states, assuming that the differential conductance of the surface states is independent of the buckling type. The bulk bands have an energetic offset of -67.6 meV between the domains with positive and negative buckling. As we use the bulk bands as reference, we shift the dI/dV spectrum from the negatively

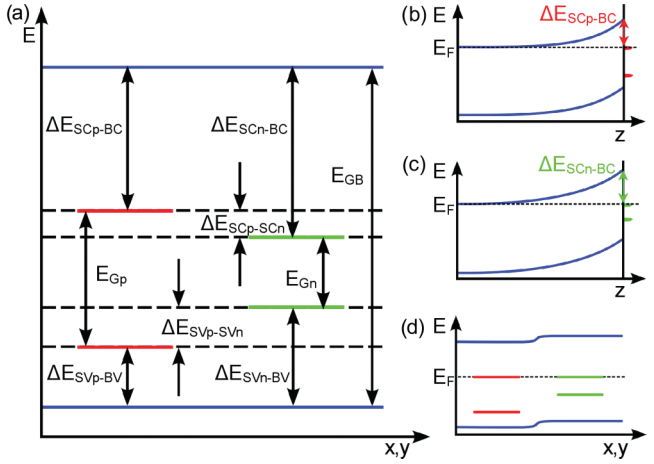

FIG. 7. (Color online) (a) Sketch of the relative energetic positions of bulk and surface bands. (b), (c) Band bending of the bulk bands and resulting space charge regions for domains with positive (b) and negative (c) buckling. (d) Band positions of bulk bands (blue) and surface bands of positively (red) and negatively (green) buckled π-bonded chains and after the surface conduction bands are aligned.

buckled domain by this value in order to adjust the bulk bands to the same value.

In the second step, the energetic difference $\Delta E_{\text{SC}p-\text{SC}n}$ between the onset of the surface conduction band of the negatively buckled π-bonded chains and the onset of the surface conduction band of the positively buckled π-bonded chains is determined. This is done via a visual overlay by shifting the spectrum for negative buckling on the voltage

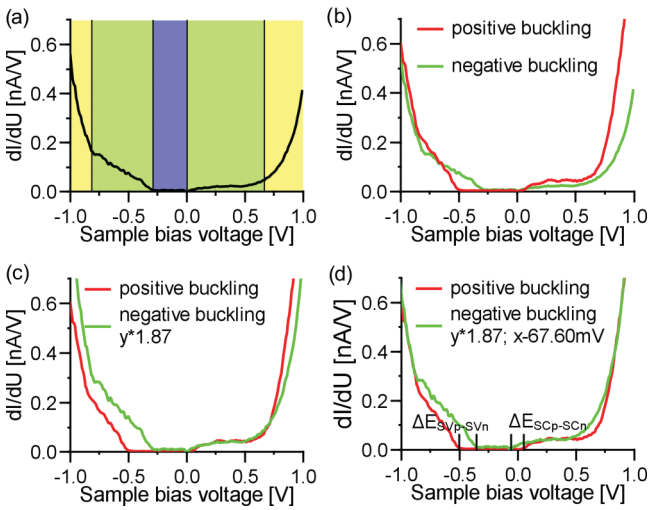

FIG. 8. (Color online) Single dI/dV spectra ($T = 6$ K). (a) Different major contributions to the tunneling current I_T: bulk valence band (BVB, yellow), bulk conduction band (BCB, yellow), surface valence band (SVB, green), and surface conduction band (SCB, green). In the band gap (BG, blue) there is no tunneling. (b)–(d) Alignment for single dI/dV spectra from positively (red line) and negatively (green line) buckled domain. (b) Original spectra, (c) multiplication of y values with 1.87 for in order to adjust dI/dV values in surface states, (d) shifting x values of spectrum from negatively buckled domain by -67.6 meV in order to align the energetic positions of bulk conduction and valence bands.

scale until the surface conduction bands of both buckling types overlay exactly. The amount of the shifting needed is $\Delta E_{\mathrm{SC}p-\mathrm{SC}n}$. This proceeding is more accurate than simple metering because there is no need to determine the exact band edge. The energetic difference $\Delta E_{\mathrm{SV}p-\mathrm{SV}n}$ between the surface valence bands is determined likewise. We find the surface bands of the π-bonded chains with negative buckling within the band gap of the π-bonded chains with positive buckling with $\Delta E_{\mathrm{SV}p-\mathrm{SV}n} = 129\,(10)$ mV and $\Delta E_{\mathrm{SC}p-\mathrm{SC}n} = 99\,(10)$ mV. These values are in excellent agreement with our calculations where we get $\Delta E^t_{\mathrm{SV}p-\mathrm{SV}n} = 87$ mV and $\Delta E^t_{\mathrm{SC}p-\mathrm{SC}n} = 85$ mV. While these values can be determined with high precision, the determination of the exact position of the surface bands within the bulk band gap is less exact. This is due to the fact that the band edges of the bulk bands are concealed by the surface bands and that the onset of tunneling into the bulk bands is smoothed. Extrapolating the course of the bulk bands in the concealed part, we get an apparent gap of 1.21 eV, which is slightly larger than the literature value $E_{GB} = 1.17$ eV at 6 K.[20] We extract $\Delta E_{\mathrm{SV}p-\mathrm{BV}} = 0.21$ eV and $\Delta E_{\mathrm{SC}p-\mathrm{BC}} = 0.51$ eV from our experimental data for positive buckling. The calculated values $\Delta E^t_{\mathrm{SV}p-\mathrm{BV}} = 0.0$ eV and $\Delta E^t_{\mathrm{SC}p-\mathrm{BC}} = 0.4$ eV ($E^t_{\mathrm{SV}} = 0.0$ eV, $E^t_{\mathrm{SC}} = 0.75$ eV, and $E^t_{\mathrm{BC}} = 1.1$ eV) differ significantly from the experimental data. This corresponds to the differences in the surface band gaps, which our experiments yield systematically smaller than found in our theory. As mentioned before, this might result from experimental difficulties in determining the center of mass of a band energy, from neglect of electron-phonon interaction in our theory, or from n-type doping. Note that the mid-gap energy of 0.36 eV (from our experiment) agrees very well with the calculated mid-gap energy of 0.38 eV.

IV. CONCLUSION

Examining domain boundaries with frontally meeting π-bonded chains, we confirm the coexistence of positive and negative buckling on Si(111)-2 × 1 at 6 K and prove this coexistence also at room temperature. CITS measurements of multidomain surfaces demonstrate spatially resolved differences in the electronic structure of different domains.

The surface bands of both buckling types are located within the band gap of bulk silicon. Single dI/dV spectra show the different band gaps for positively and negatively buckled π-bonded chains $E_{Gp} = 520$ (20) mV and $E_{Gn} = 290\,(20)$ mV, in qualitative agreement with other experiments and calculations.[8,9] We were able to determine the relative position of the surface bands of differently buckled π-bonded chains. The surface bands of the π-bonded chains with negative buckling lie within the band gap of the π-bonded chains with positive buckling and the energetic differences are $\Delta_{\mathrm{SV}p-\mathrm{SV}n} = -129$ (10) mV and $\Delta_{\mathrm{SC}p-\mathrm{SC}n} = 99\,(10)B$ mV. These results are supported by the excellent match with our calculations.

ACKNOWLEDGMENT

We acknowledge financial support by the DFG via Project No. WE 1889/3.

*wendero@gwdg.de

[1] I. Appelbaum, T. Wang, S. Fan, J. D. Joannopoulos, and V. Narayanamurti, Nanotechnology **12**, 391 (2001).
[2] K. Sagisaka, D. Fujita, and G. Kido, Phys. Rev. Lett. **91**, 146103 (2003).
[3] D. Riedel, M. Lastapis, M. G. Martin, and G. Dujardin, Phys. Rev. B **69**, 121301 (2004).
[4] Y. Takagi, Y. Yoshimoto, K. Nakatsuji, and F. Komori, Surf. Sci. **559**, 1 (2004) .
[5] K. Sagisaka and D. Fujita, Phys. Rev. B **71**, 245319 (2005).
[6] K. Seino, W. G. Schmidt, and F. Bechstedt, Phys. Rev. Lett. **93**, 036101 (2004).
[7] J. Nakamura and A. Natori, Phys. Rev. B **71**, 113303 (2005).
[8] S.-H. Lee and M.-H. Kang, Phys. Rev. B **54**, 1482 (1996).
[9] G. Bussetti, B. Bonanni, S. Cirilli, A. Violante, M. Russo, C. Goletti, P. Chiaradia, O. Pulci, M. Palummo, R. Del Sole *et al.*, Phys. Rev. Lett. **106**, 067601 (2011).
[10] K. C. Pandey, Phys. Rev. Lett. **47**, 1913 (1981).
[11] S. Nie, R. M. Feenstra, J. Y. Lee, and M.-H. Kang, J. Vac. Sci. Technol. A **22**, 1671 (2004).
[12] M. Rohlfing, M. Palummo, G. Onida, and R. Del Sole, Phys. Rev. Lett. **85**, 5440 (2000).
[13] J. K. Garleff, M. Wenderoth, K. Sauthoff, R. G. Ulbrich, and M. Rohlfing, Phys. Rev. B **70**, 245424 (2004).
[14] F. J. Himpsel, G. Hollinger, and R. A. Pollak, Phys. Rev. B **28**, 7014 (1983).
[15] J. A. Stroscio, R. M. Feenstra, and A. P. Fein, Phys. Rev. Lett. **57**, 2579 (1986).
[16] M. Rohlfing and J. Pollmann, Phys. Rev. Lett. **88**, 176801 (2002).
[17] J. K. Garleff, M. Wenderoth, R. G. Ulbrich, C. Sürgers, and H. v. Löhneysen, Phys. Rev. B **72**, 073406 (2005).
[18] A. K. Ramdas and S. Rodriguez, Rep. Prog. Phys. **44**, 1297 (1981).
[19] R. M. Feenstra and J. A. Stroscio, J. Vac. Sci. Technol. B **5**, 923 (1987).
[20] W. Bludau, A. Onton, and W. Heinke, J. Appl. Phys. **54**, 1846 (1974).